Built on LDRD Laboratory Directed Research and Development

SAND20XX-XXXXR

LDRD PROJECT NUMBER: 173868

LDRD PROJECT TITLE: Modeling of Nonlocal Electron Conduction for Inertial Confinement Fusion

PROJECT TEAM MEMBERS: Jeffrey Chenhall, University of Wisconsin

ABSTRACT:

In this report Chenhall presents a new Monte Carlo (MC) transport method developed as part of his PhD thesis work funded via fellowship by Sandia National Laboratories. The model is used to simulate the electron thermal transport within inertial confinement fusion (ICF) type problems. The new model aims to improve upon the currently used implicit Schurtz, Nicolai, and Busquet (iSNB) method [1][2], in particular by using finite particle ranges in comparison to the exponential solution of a diffusion method and by improved higher order angular modeling. The new method is being developed using the 1D LILAC and 2D DRACO codes developed by the Rochester Laboratory for Laser Energetics. The model is compared to iSNB for several ICF type problems: Omega shot 60303 a shock timing experiment [3], Omega shot 68951 a cryo target implosion [4] and a NIF phase plate polar direct drive design [5]. Overall, the MC method performs at least as well as the iSNB method and appears to indicate a lower predicted preheat ahead of the shock fronts. However, the difference in overall results between iSNB and MC transport is small for the choice of test problems and further simulations will need to be run to fully understand the difference between the models.

INTRODUCTION:

The research is in collaboration with the University of Wisconsin-Madison (UW). This research aims to advance modeling of non-local electron thermal conduction, an important Inertial Confinement Fusion (ICF) phenomenon, for direct drive ICF target implosions. Current capability involves multi-group diffusion based theory of "diffusing" higher order moments of the electron distribution function to simulate non-local electron thermal conduction. In this research, a new Monte Carlo (MC) transport method is developed to efficiently simulate non-local electron thermal conduction. The work involves model development in the 1D LILAC and 2D DRACO radiation hydrodynamics simulation codes developed by the Laboratory for Laser Energetics (LLE), Rochester, New York.

Background:

The numerical simulation of heat transport throughout the plasma is important for providing predictive capability for ICF experiments. The Spitzer-Harm (SH) heat flux arises from a first order angular expansion of the electron distribution function $f(\mathbf{r}, v, \mathbf{\Omega}) = f_0(\mathbf{r}, v) + 3\mathbf{\Omega} \cdot \mathbf{f}_1(\mathbf{r}, v)$ where f_0 is the Maxwell-Boltzmann distribution [6]. Starting with the Boltzmann transport equation Spitzer derived an expression for the electron heat conduction:

$$\mathbf{Q}_{SH} = -K_{SH} \nabla T_e \quad (1)$$

where $\mathbf{Q}_{SH}$ is the electron heat flux, T_e is the electron temperature, and K_{SH} is Spitzer heat conductivity. Spitzer theory is based upon the assumption that the distribution function is primarily Maxwellian with a small higher angular order correction term. Consequently the Spitzer result is most applicable where the ratio f_1/f_0 is small or equivalently the length scale of the temperature gradient $|T_e/\nabla T_e|$ greatly exceeds the electron mean free path (MFP) length.

Shortcomings arise in Spitzer theory when applied to high energy density physics (HEDP) problems such as ICF. When applied to a shockwave in an ICF implosion, the heat in front of the wave (the preheat) is underpredicted and the heat flux and speed of the shockwave are overpredicted. Preheating is important because it conditions the material ahead the shockwave affecting its propagation. The reason for the underprediction of electron preheating is because high energy electrons have a greater MFP than the temperature scale length. This allows electrons to stream out ahead of the shockwave/gradient region and contribute to the preheating. Since the Spitzer heat flux only depends on the local temperature gradient, the high energy electrons remain in the wave front accounting for the underprediction of the preheat and overprediction of the heat flux. The overprediction of the heat flux results in the shockwave propagating with a too high velocity. Traditionally, to combat the overprediction of heat flux a flux limiter model is often invoked. The heat flux is capped at a maximum value proportional to the electron thermal velocity via

$$Q_{fl} = \min|Q_{SH}, \alpha n_e v_{th}| \tag{2}$$

where α is the flux limiter n_e is the electron density, and v_{th} is the electron thermal velocity. The flux limiter is a user defined parameter that is commonly set to 0.06 due to agreement with past experimental data. The underprediction of preheat still remains a problem even with a flux limiter and higher fidelity model is needed to properly model it.

Due to these shortcomings of the Spitzer solution Luciani, Mora and Virmont (LMV) propose a convolution kernel modification to the Spitzer flux to take into account long MFP behavior near strong temperature gradients [7]. The kernel takes into account the energy dependence of an electron's MFP length and acts to delocalize the Spitzer flux, essentially allowing for higher energy electrons to escape the local temperature gradient. The modification involves the convolution of the delocalization kernel with the Spitzer flux expression via

$$Q(x) = \int_{-\infty}^{\infty} W(x,x') Q_{SH} \frac{dx'}{a\lambda_e(x')} \tag{3}$$

where $Q(x)$ is the non-local heat flux, $W(x,x')$ is the delocalization kernel, a is an adjustable parameter with a recommended value of 32, and λ_e is the electron MFP length. The kernel takes the form

$$W(x,x') = \beta \exp\big(-\tau(x,x')\big) \tag{4}$$

where β is a normalization constant and $\tau(x,x')$ is a measure of optical depth between points x and x' given by

$$\tau(x,y) = \frac{\left|\int_x^y n_e(z)dz\right|}{a n_e(y)\lambda_e(y)}. \tag{5}$$

For small MFP lengths relative to the temperature gradient length scale the kernel behaves as a delta function and the Spitzer heat flux relation is recovered. The expression can be generalized to multiple dimensions by replacing x, x' by $\mathbf{r}$ and $\mathbf{r} + s\boldsymbol{\Omega}$ respectively and integrating over $\mathbb{R}^3$ via

$$\mathbf{Q}(\mathbf{r}) = \int_{4\pi} \boldsymbol{\Omega}\boldsymbol{\Omega} \mathrm{d}^2\Omega \int_0^\infty W_0(\mathbf{r}, \mathbf{r} + s\boldsymbol{\Omega}) \mathbf{Q}_{SH}(\mathbf{r} + s\boldsymbol{\Omega}) \frac{ds}{\lambda_e(\mathbf{r} + s\boldsymbol{\Omega})} \tag{6}$$

where W_0 is the 1D kernel.

Schurtz, Nicolai, and Busquet (SNB) note that the LMV non-local flux looks like the integral solution of a transport equation [1]. SNB define $q(\boldsymbol{\Omega}, \mathbf{r})$as the angular flux solution of the linear steady state transport equation

$$\boldsymbol{\Omega} \cdot \boldsymbol{\nabla} q(\boldsymbol{\Omega}, \mathbf{r}) = \frac{1}{\lambda_t(\mathbf{r})} \left(\frac{3}{4\pi} \boldsymbol{\Omega} \cdot \mathbf{Q}_{SH}(\mathbf{r}) - q(\boldsymbol{\Omega}, \mathbf{r}) \right). \tag{7}$$

The solution to this equation is

$$q(\boldsymbol{\Omega}, \mathbf{r}) = \frac{3}{4\pi} \int_0^\infty \exp\left(-\tau(\mathbf{r}, \mathbf{r} - s\boldsymbol{\Omega})\right) \boldsymbol{\Omega} \cdot \mathbf{Q}_{SH}(\mathbf{r} - s\boldsymbol{\Omega}) \frac{ds}{\lambda_t(\mathbf{r} - s\boldsymbol{\Omega})} \tag{8}$$

where τ is the optical depth

$$\tau(\mathbf{r}, \mathbf{r}') = \int_{\mathbf{r}}^{\mathbf{r}'} \frac{dr''}{\lambda_t(\mathbf{r}'')}. \tag{9}$$

Taking the first angular moment of the angular flux yields the heat flux expression (6) with delocalization kernel

$$W_0(\mathbf{r}, \mathbf{r}') = \exp(-\tau(\mathbf{r}, \mathbf{r}')). \tag{10}$$

Due to differing plasma conditions between an electron's start and end point the delocalization kernel will be non-symmetric. In order to mitigate computational issues associated with a non-symmetric kernel SNB propose a multigroup approach. By splitting into energy groups (7) becomes

$$\boldsymbol{\Omega} \cdot \boldsymbol{\nabla} q_g(\boldsymbol{\Omega}, \mathbf{r}) = \frac{1}{\lambda_g(\mathbf{r})} \left(\frac{3}{4\pi} \boldsymbol{\Omega} \cdot \mathbf{U}_g(\mathbf{r}) - q_g(\boldsymbol{\Omega}, \mathbf{r}) \right) \tag{11}$$

where $\mathbf{U}_g(\mathbf{r})$ is the multigroup source term

$$\mathbf{U}_g = \frac{1}{24} \int_{E_{g-1}/kT}^{E_g/kT} \beta^4 e^{-\beta} \mathbf{Q}_{SH} \mathrm{d}\beta \tag{12}$$

and λ_g is the multigroup MFP

$$\lambda_g = 2\left(E_{g-1/2}/kT\right)^2 \lambda_e.$$

Taking the first two angular moments of (11) and combining to get a diffusion equation gives

$$\left(\frac{1}{\lambda_g(\mathbf{r})} - \nabla \frac{\lambda_g(\mathbf{r})}{3} \nabla \right) H_g(\mathbf{r}) = -\boldsymbol{\nabla} \cdot \mathbf{U}_g(\mathbf{r}) \tag{13}$$

where $H_g(\mathbf{r})$ is the zeroth angular moment of $q_g(\boldsymbol{\Omega}, \mathbf{r})$. The heat flux is then given by

$$\mathbf{Q}_{\mathrm{SNB}}(\mathbf{r}) = \mathbf{Q}_{SH}(\mathbf{r}) - \sum_g \frac{\lambda_g(\mathbf{r})}{3} \nabla H_g(\mathbf{r}) \tag{14}$$

where it is readily apparent that the SNB method produces a correction term to the Spitzer flux. Note that in the short MFP limit the SNB heat flux reduces to the Spitzer result. To give physical meaning to the quantity $H_g(\mathbf{r})$, SNB propose an alternative derivation starting from the steady state Fokker-Planck equation. Through this derivation it is found that

$$H(\mathbf{r}, v) = \frac{1}{2} m_e v^5 \Delta f_0(\mathbf{r}, v) \tag{15}$$

where $\Delta f_0(\mathbf{r}, v)$ is the non-Maxwellian correction to the zeroth order angular moment to the electron distribution function.

Cao et. al. have worked to improve upon the original method developed in Schurtz et. al., developing an improved implicit SNB (iSNB) algorithm for use in the DRACO code [1][2]. In order to advance the system in time, the SNB method is coupled to the electron temperature equation

$$\rho C_v \frac{\partial T_e}{\partial v} = -\nabla \cdot \mathbf{Q} + S_{ext} \tag{16}$$

where ρ is the density, C_v is the specific heat, $\mathbf{Q}$ is the heat flux, and S_{ext} is some external source term. Starting at a time step *n* the iSNB algorithm solves iteratively for the updated temperature at the next time step *n+1*. In contrast to SNB's original algorithm, which solves explicitly for $\mathbf{Q}_{\mathrm{nl}}$, the iSNB algorithm solves for the easier to compute $\nabla \cdot \mathbf{Q}_{nl}$ which is directly used in the temperature equation. The iterative algorithm is as follows:

1. Solve the temperature equation for T_e^k
$$\rho C_v \frac{T_e^k - T_e^n}{\Delta t} = -\nabla \cdot \mathbf{Q}_{SH}^k + S_{ext}^n + S_{nl,correction}^{k-1} \tag{17}$$
where *k* is the iterative index, $\mathbf{Q}_{SH}^k = -K_{SH}^k \nabla T_e^k$, $S_{nl,correction}^{k-1}$ is the SNB correction to the Spitzer flux divergence, and $S_{nl,correction}^0 = 0$.
2. Recompute $\nabla \cdot \mathbf{Q}_{SH}^k$ using T_e^k
3. If k>1, check for convergence with criterion
$$\left|\nabla \cdot \mathbf{Q}_{SH}^k - \nabla \cdot \mathbf{Q}_{SH}^{k-1}\right| \leq \alpha \rho C_{v,e} \frac{T_e^k}{\Delta t} \tag{18}$$
where α is a user defined parameter set to 0.01. If converged, set $T_e^{n+1} = T_e^k$ and exit the loop advancing to the next time step.
4. If not converged, solve the SNB diffusion equation
$$\left(\frac{1}{\lambda_g(\mathbf{r})} - \nabla \frac{\lambda_g(\mathbf{r})}{3} \nabla\right) H_g^k(\mathbf{r}) = \nabla \cdot \left(\frac{K_{SH}^k \nabla T_e^k}{24} \int_{\beta_{g-1}}^{\beta_g} \beta^4 e^{-\beta} \mathrm{d}\beta\right) = -\nabla \cdot \mathbf{U}_g^k(\mathbf{r}) \tag{19}$$
where g is the group index and $\beta_g = E_g / kT$.
5. Compute
$$-\nabla \cdot \mathbf{Q}_{nl}^k = \sum_g \frac{H_g^k}{\lambda_g^k} \tag{20}$$

6. Compute

$$S^k_{nl,correction} = -\nabla \cdot \mathbf{Q}^k_{nl} + \nabla \cdot \mathbf{Q}^k_{SH} \tag{21}$$

7. Repeat from step 1 for the next iteration of k.

The MFP formula in the original SNB paper assumes plasma conditions which leads to inaccuracies, particularly too high of preheating at low temperatures. Cao recommends the use of a range formula by Atzeni, Schiavi, and Davies

$$\frac{d\mathcal{E}}{\rho ds} = -\frac{D}{\beta^2} \tag{22}$$

where

$$D = \frac{4\pi e^4}{m_p m_e c^2}\frac{Z}{A}\left[\ln\frac{m_e c^2}{\hbar\omega_{pe}} + \frac{9}{16} - \frac{1}{2}\ln 2 + f(\gamma)\right] \tag{23}$$

$$f(\gamma) = \ln\left(\beta\sqrt{\gamma - 1}\right) - \frac{(1/8) + \ln 2}{\gamma} + \frac{(1/16) + (1/2)\ln 2}{\gamma^2} \tag{24}$$

where m_p is the proton mass, $\hbar$ is the reduced Planck constant, $\omega_{pe} = \sqrt{4\pi n_e e^2/m_e}$ is the electron-plasma frequency, n_e is the electron density, γ is the Lorentz factor, and β is the ratio of velocity to the speed of light [8]. The range is computed by integrating $d\varepsilon/ds$ over distance in the direction of the origin. Currently, the iSNB method is being used to simulate electron thermal transport in the 1D LILAC and 2D DRACO Multiphysics codes developed at LLE. Chenhall aims to improve upon the iSNB method with his MC transport method described in the following section.

DETAILED DESCRIPTION OF EXPERIMENT/METHOD:

The derivation of the new method begins with the steady state Fokker-Planck equation

$$\mathbf{v} \cdot \nabla f - \frac{e\mathbf{E}}{m_e}\frac{\partial f}{\partial \mathbf{v}} = C(f) \tag{25}$$

where f is the electron distribution function, $\mathbf{v}$ is the electron velocity, $\mathbf{E}$ is the electric field, and $C(f)$ is the collision operator. The distribution function is expanded in terms of a first angular order Maxwellian solution and a correction term.

$$f(\mathbf{r}, \boldsymbol{v}, \boldsymbol{\Omega}) = f_0^{mb}(\mathbf{r}, \boldsymbol{v}) + 3\boldsymbol{\Omega} \cdot \mathbf{f}_1^{mb}(\mathbf{r}, \boldsymbol{v}) + \Delta f(\mathbf{r}, \boldsymbol{v}, \boldsymbol{\Omega}) \tag{26}$$

Plugging this expansion into the transport equation gives:

$$\begin{aligned} 0 = {} & C\left(\Delta f(\mathbf{r}, \boldsymbol{v}, \boldsymbol{\Omega})\right) + v\boldsymbol{\Omega} \cdot \nabla\left(\Delta f(\mathbf{r}, \boldsymbol{v}, \boldsymbol{\Omega})\right) - \frac{e\mathbf{E}}{m_e} \cdot \frac{\partial\left(\Delta f(\mathbf{r}, \boldsymbol{v}, \boldsymbol{\Omega})\right)}{\partial \mathbf{v}} \\ & + \left[C\left(f_0^{mb}(\mathbf{r}, \boldsymbol{v})\right)\right] \\ & + \left[C\left(3\boldsymbol{\Omega} \cdot \mathbf{f}_1^{mb}(\mathbf{r}, \boldsymbol{v})\right) + v\boldsymbol{\Omega} \cdot \nabla\left(f_0^{mb}(\mathbf{r}, \boldsymbol{v})\right) - \frac{e\mathbf{E}}{m_e} \cdot \boldsymbol{\Omega}\frac{\partial f_0^{mb}(\mathbf{r}, \boldsymbol{v})}{\partial v}\right] \\ & + v\boldsymbol{\Omega} \cdot \nabla\left(3\boldsymbol{\Omega} \cdot \mathbf{f}_1^{mb}(\mathbf{r}, \boldsymbol{v})\right) - \frac{3e\mathbf{E}}{m_e v^2} \cdot \frac{\partial\left(v^2 \mathbf{f}_1^{mb}(\mathbf{r}, \boldsymbol{v})\right)}{\partial v} \end{aligned} \tag{27}$$

The two expressions in square brackets are both equal to zero. The first since collisions of a Maxwellian are in equilibrium and the second by the definition of the $\mathbf{f}_1^{mb}$ quantity. Furthermore, we make the assumption that the collision operator is well approximated by a collision frequency times the distribution function. This simplifies the transport equation to:

$$C(\Delta f) + v\boldsymbol{\Omega}\cdot\boldsymbol{\nabla}(\Delta f) - \frac{e\mathbf{E}}{m_e}\cdot\frac{\partial(\Delta f)}{\partial \mathbf{v}} = -3v\boldsymbol{\Omega}\cdot\boldsymbol{\nabla}\left(\boldsymbol{\Omega}\cdot\mathbf{f}_1^{mb}\right) + \frac{3e\mathbf{E}}{m_e v^2}\cdot\frac{\partial\left(v^2\mathbf{f}_1^{mb}\right)}{\partial v} \tag{28}$$

The equation is further simplified by multiplying through by $\frac{1}{2}m_e v^5$ (v^3 for the heat flux and v^2 for the Jacobian factor for the velocity integral), neglecting the electric field term, and assuming the source term has the same functional form in velocity as the SNB model. Collecting the $\frac{1}{2}m_e v^5\Delta f$ terms puts the equation in terms of the correction to the angular dependent heat flux $\Delta q(\mathbf{r}, v, \boldsymbol{\Omega})$.

$$\frac{1}{\lambda(\mathbf{r}, v)}\,\Delta q(\mathbf{r}, v, \boldsymbol{\Omega}) + \boldsymbol{\Omega}\cdot\boldsymbol{\nabla}\left(\Delta q(\mathbf{r}, v, \boldsymbol{\Omega})\right) = -3\boldsymbol{\Omega}\cdot\boldsymbol{\nabla}\left(g(v)\boldsymbol{\Omega}\cdot\mathbf{Q}_{SH}(\mathbf{r})\right) \tag{29}$$

where

$$g(v) = \frac{1}{12v_{th}}\left(\frac{v}{v_{th}}\right)^9 \exp(-(v/v_{th})^2) \tag{30}$$

Note that the source term on the RHS of the transport equation (29) is equivalent to the 0th angular order SNB source term plus a second angular order term. The non-local heat flux $\mathbf{Q}_{nl}$ is related to Δq via

$$\mathbf{Q}_{nl} = \mathbf{Q}_{SH} + \int_0^\infty\int_{4\pi}\Delta q(\mathbf{r}, v, \boldsymbol{\Omega})\boldsymbol{\Omega}\mathrm{d}\boldsymbol{\Omega}\mathrm{d}v \tag{31}$$

or alternatively

$$\boldsymbol{\nabla}\cdot\mathbf{Q}_{nl} = \boldsymbol{\nabla}\cdot\mathbf{Q}_{\mathrm{SH}} - \int_0^\infty\int_{4\pi}\frac{\Delta q(\mathbf{r}, v, \boldsymbol{\Omega})}{\lambda(\mathbf{r}, v)} - 3\boldsymbol{\Omega}\cdot\boldsymbol{\nabla}\left(g(v)\boldsymbol{\Omega}\cdot\mathbf{Q}_{SH}(\mathbf{r})\right)\mathrm{d}\boldsymbol{\Omega}\mathrm{d}v \tag{32}$$

$$\boldsymbol{\nabla}\cdot\mathbf{Q}_{nl} = -\int_0^\infty\int_{4\pi}\frac{\Delta q(\mathbf{r}, v, \boldsymbol{\Omega})}{\lambda(\mathbf{r}, v)}\mathrm{d}\boldsymbol{\Omega}\mathrm{d}v \tag{33}$$

The $\boldsymbol{\nabla}\cdot\mathbf{Q}_{nl}$ quantity can then be used in the iSNB temperature update algorithm.

The transport equation (29) is solved via the following algorithm.

- Energy is treated group-wise for the purpose of calculating mfps and slowing down quantities.
- Electron MC particles (MCP) in each cell/energy group are allocated in proportion to source magnitude $\left|\boldsymbol{\nabla}\cdot\mathbf{U}_g(\mathbf{r})\right|$, where $\mathbf{U}_g$ is the group-wise component of the Spitzer flux.
- For each MCP:
  - Direction Ω is sampled uniformly over 4π.
  - Particle starting position is sampled uniformly in volume within its starting cell.
  - The initial MCP energy is sampled from the distribution $(v/v_{th})^9\exp(-(v/v_{th})^2)$
  - Particle begins with an initial weight $-3\boldsymbol{\Omega}\cdot\boldsymbol{\nabla}\left(g(v)\boldsymbol{\Omega}\cdot\mathbf{Q}_{SH}(\mathbf{r})\right)\big|_{cell,\ g}$
- For the transport of the particle

- Distance to boundary, collision, and downscattering interactions are computed and the closest interaction is selected.
- MCP weight is reduced by a factor of $\exp\left(-d_{min}/\lambda_g(\mathbf{r})\right)$ with the difference added to the current cell's tally.
- If a downscattering interaction occurs the group index is decremented.
- Particle history is terminated when either the particle weight falls below a fixed fraction of its initial weight or its energy is depleted with any remaining particle weight added to the current cells tally.

Simulations:

The model was tested against several simulations in both the 1D LILAC and 2D DRACO codes against currently existing methods in the code, the iSNB diffusion method.

1D Simulations:

Shock timing experiment Omega shot 60303:

Shot 60303 was a cryogenic target shot on LLE's OMEGA laser system [3]. The primary purpose of this experiment was to measure the shock convergence within a target. Shock velocity was measured using a Velocity Interferometer System for Any Reflector (VISAR) device on which the target was mounted (Figure 1). The target consisted of a CD shell and an inner liquid deuterium layer. The laser profile consisted of three laser pickets followed by a main drive (Figure 2). Since each laser picket is successively larger the shocks catch up to each other at which point there is a marked increase in the shock velocity.

Simulation of this shot was done in LLE's 1D LILAC code, the simulation in 1D spherical geometry consisted of an innermost 23.5 micron thick 10 cell region of DD gas at $4.5\text{x}10^{-4}$ g/cm^3 density, followed by a middle layer of 400 micron thick 400 cell region of DD liquid at 0.17 g/cm^3 density, and an outermost 9.5 micron thickness layer consisting of 220 cell region of deuterated plastic at density 0.985 g/cm^3 (Figure 3).

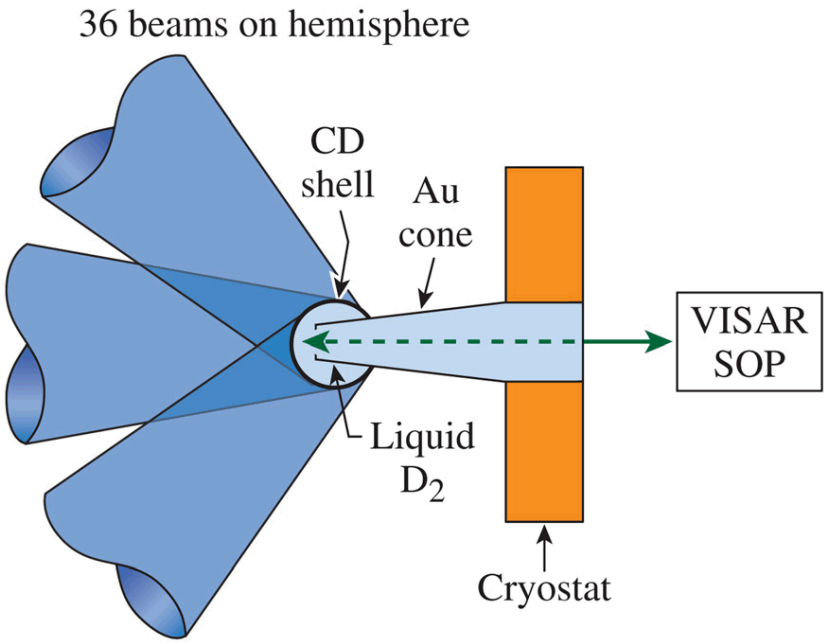

Figure 1. Diagram depicting the experimental setup for the Omega shot 60303 shock timing experiment. 36 beams illuminate a hemisphere of the target. [Image from Boehly 2011 [3]]

.

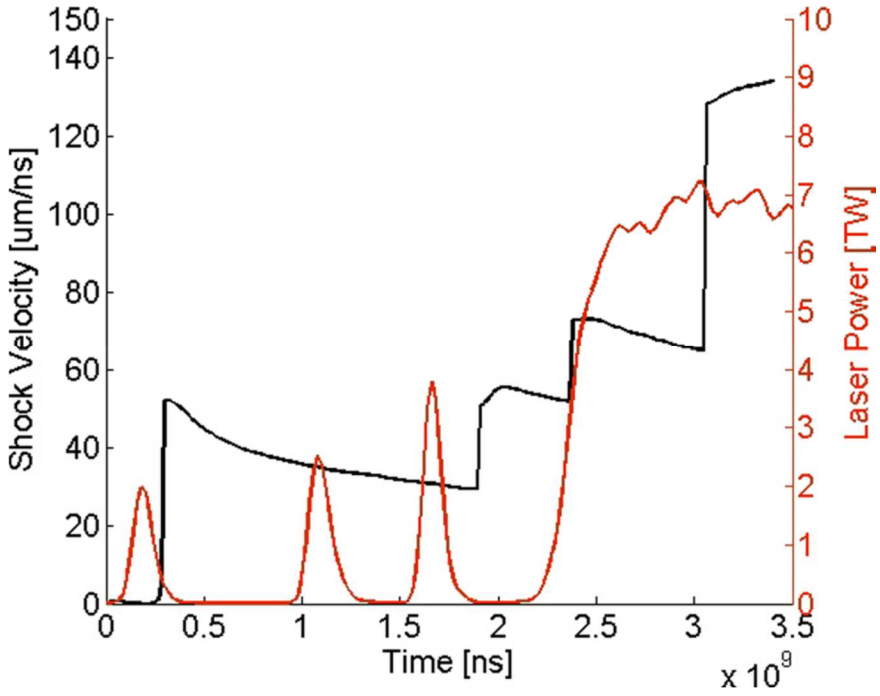

Figure 2. Measured shock velocity (black) and laser power (red) for Omega shot 60303. [Image from Cao 2015 [2]]

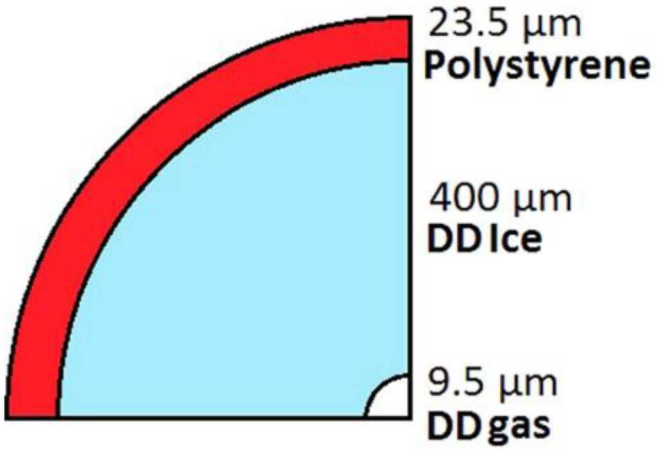

Figure 3. Cross section of fuel capsule for Omega shot 60303 [Image from Cao 2015 [2]]

***Cryogenic target implosion experiment Omega shot 68951*:**
Simulation of this shot was done in LLE's 1D LILAC code [4]. The simulation in 1D spherical geometry consisted of an innermost 379 micron thick 150 cell region of DT gas (41.16% tritium) at 6.8×10^{-4} g/cm^3 density, followed by a middle layer of 47 micron thick 300 cell region of DT

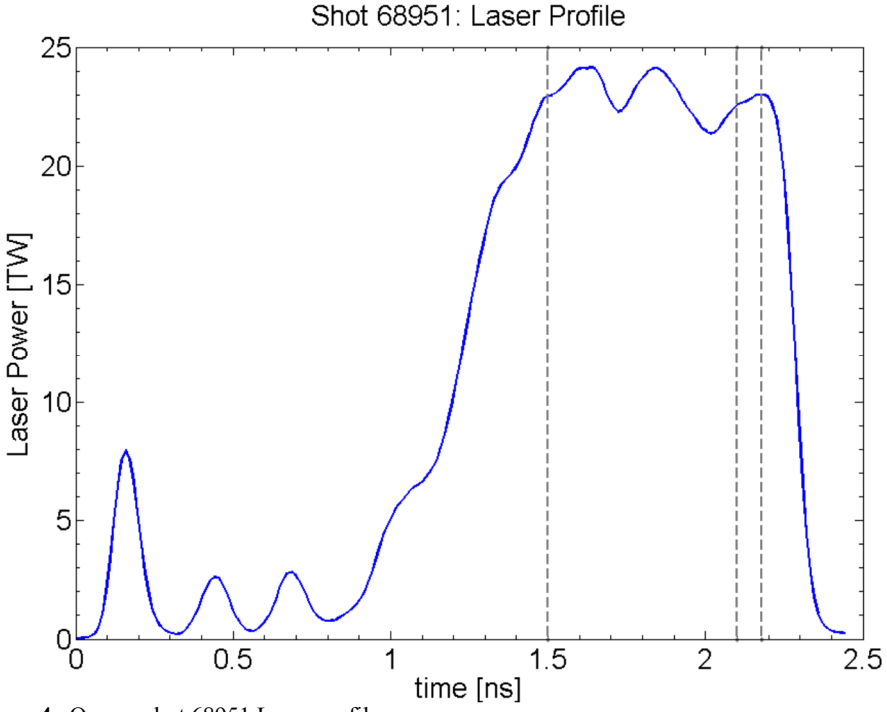

Figure 4. Omega shot 68951 Laser profile.

ice (43% tritium) at 0.237g/cm^3 density, and an outermost 8.4 micron thickness layer consisting of 100 cell region of deuterated plastic at density 1.08g/cm^3. The laser profile consisted of three picket laser pulses followed by a main drive for a total laser energy of 26.9 kJ (Figure 4).

2D Simulations:

***Shock timing experiment Omega shot 60303*:**

The 2D simulation of shot 60303 consisted of a wedge in RZ coordinates consisting of the same configuration as the 1D simulation in the radial direction and 10 cells in the transverse direction with reflective boundary conditions along the edge of the cone.

NIF phase plate polar direct drive design [5]:

The Phase Plate target design produced by LLE is an example of a direct drive ICF shot that could be fielded on the NIF laser system. Since NIF is designed to illuminate indirect drive hohlraum targets the beams are positioned towards the poles of the target. As such if a direct drive target were to be shot on NIF the laser drive would require balancing to account for the non-ideal laser positioning (Figure 5). The laser profile for this simulation consists of two laser pickets followed by a main drive pulse for a total of 700 kJ of laser power (Figure 6).

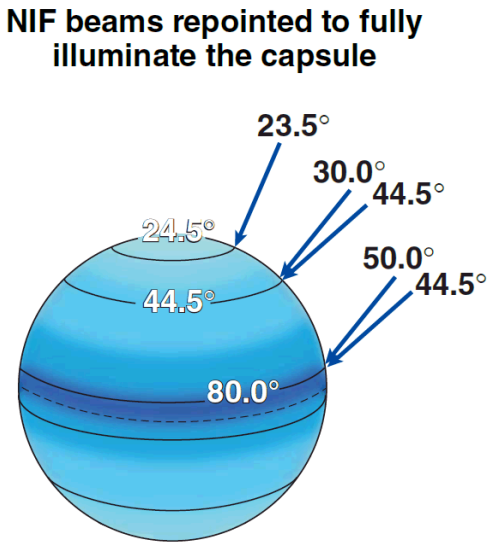

Figure 5. Example of laser pointing scheme for polar direct drive illumination at NIF [Image from Collins 2012 [9]]

Radially the simulation consists of an innermost DD gas region at 15 atmosphere pressure 400 microns in radius consisting of 40 cells; this is followed by a DD gas region at 15 atmosphere pressure, 820 microns thick consisting of 87 cells; this is followed by a plastic (CH) solid

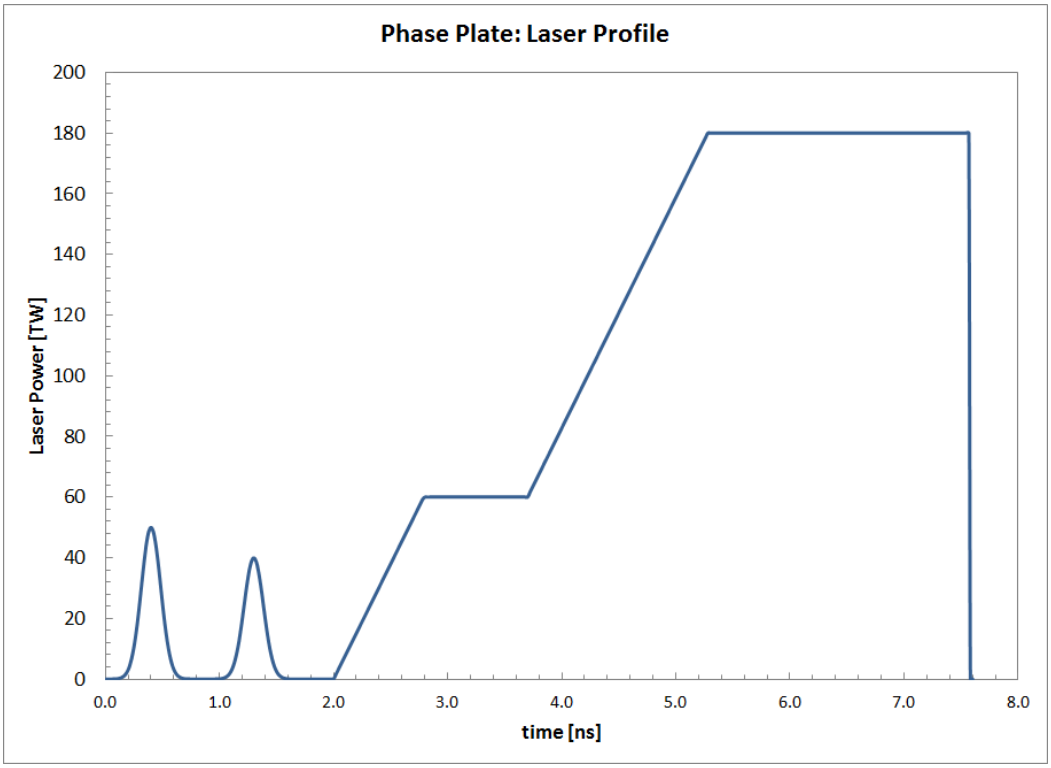

Figure 6. NIF phase plate laser profile consisting of two pickets and a ramp up to full power. [5]

ablation layer at 1.03 g/cm^3 density 79.85 microns thick consisting of 130 cells; and an outmost CH ablation layer at 1.03 g/cm^3 density, 0.15 microns thick consisting of 2 cells. In the transverse direction the simulation consists of 90 equally spaced cells.

RESULTS:

The integrated results of these simulations indicate that the diffusion based iSNB method is adequate for these experimental conditions. This is because the MC transport method yields similar results to the iSNB method.

1D: Simulations:

***Shock timing experiment Omega shot 60303*:**

The 1D Omega shot 60303 simulation was run with three methods in the LLE's 1D LILAC multiphysics code: the iSNB method, Chenhall's new MC transport method and a third 1D method by Valeri Goncharov [10]. The simulations were run on a single core as LILAC is a non-parallelized code. The MC transport model was run with run with 2.5x10^6 MCP per time step which is an average of about 100 MCP per cell group. Simulations seem to indicate that an average of 10 MCP per cell group is sufficient for a convergent solution of the $\nabla \cdot \mathbf{Q}_{nl}$ quantity. Note that since many of the cells fall outside of the gradient region they have a low importance to calculating the solution and as such have less than the average number of MCP. Since $\nabla \cdot \mathbf{Q}_{nl}$

is orders of magnitude larger nearest to the material gradients the low number of MCP in the other cells (and resultant higher variance) does not affect the overall solution.

The three models were run to 3.5 ns and the shock front position was extracted from the code as the innermost point where the density had risen to about 2 times its initial density. The shock velocity was computed via the numerical derivative of the shock position. The shock velocity was compared between models and against the experimental VISAR measurement (Figure 7). The MC transport and iSNB shock timing curves are the closest together and the Goncharov method most closely matches the experimental model.

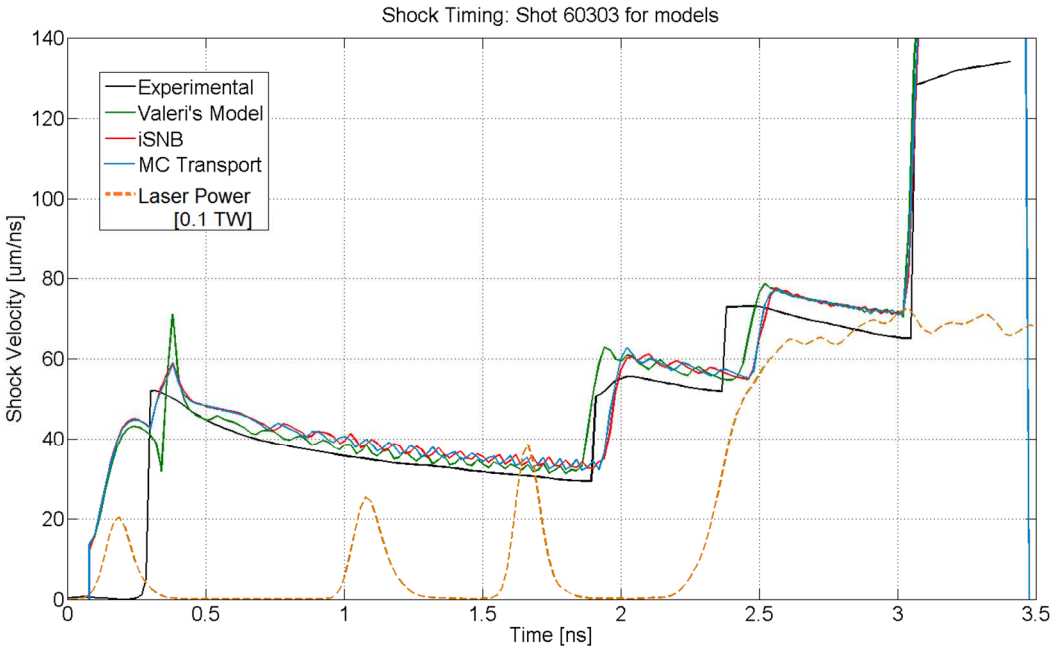

Figure 7. Shock timing comparison in μm/ns for iSNB, Chenhall's MC transport and Goncharov electron thermal transport methods with the experimental VISAR data [3].

***Cryogenic target implosion experiment Omega shot 68951*:**
The 1D Omega shot 68951 simulation was run with Chenhall's MC transport method, the iSNB method and Goncharov's method. The MC transport model was run using $2x10^5$ MCP per time step. The electron temperature and density profiles were compared at a number of time steps. The time steps chosen to display are at 1.5ns when the laser initially hits full power (Figure 8), 2.1ns near the end of main laser drive (Figure 9), and 2.18ns at the bang time of the implosion (figure adiabat). For each time step the MC transport solution most resembles the iSNB solution. One important figure of merit to ICF implosions is the adiabat (defined as pressure divided by the Fermi pressure), which is a measure of idealness of the capsule's compression. Often this is quoted as a singular number for an implosion, taken to be the minimum value of the adiabat in the high density shell at bang time. The MC transport simulation had an adiabat of 3.798, the iSNB had 3.874, and the Goncharov had 3.941 (Figure 10).

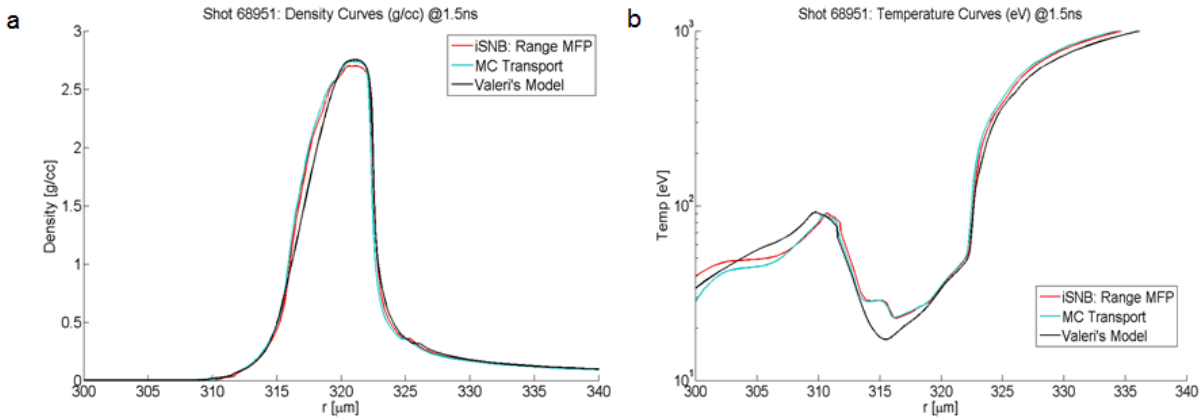

Figure 8. Shot 68951 density (a) and electron temperature (b) profiles at 1.5ns.

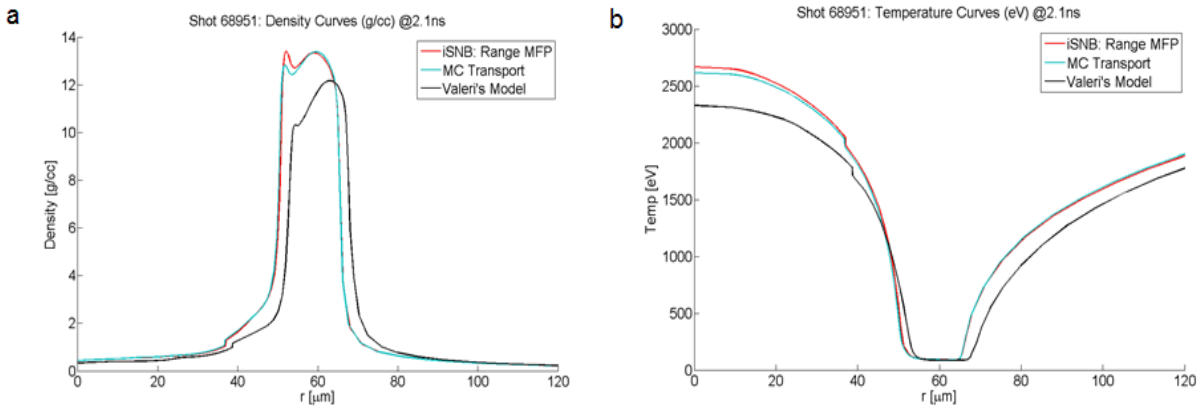

Figure 9. Shot 68951 density (a) and electron temperature (b) profiles at 2.1ns.

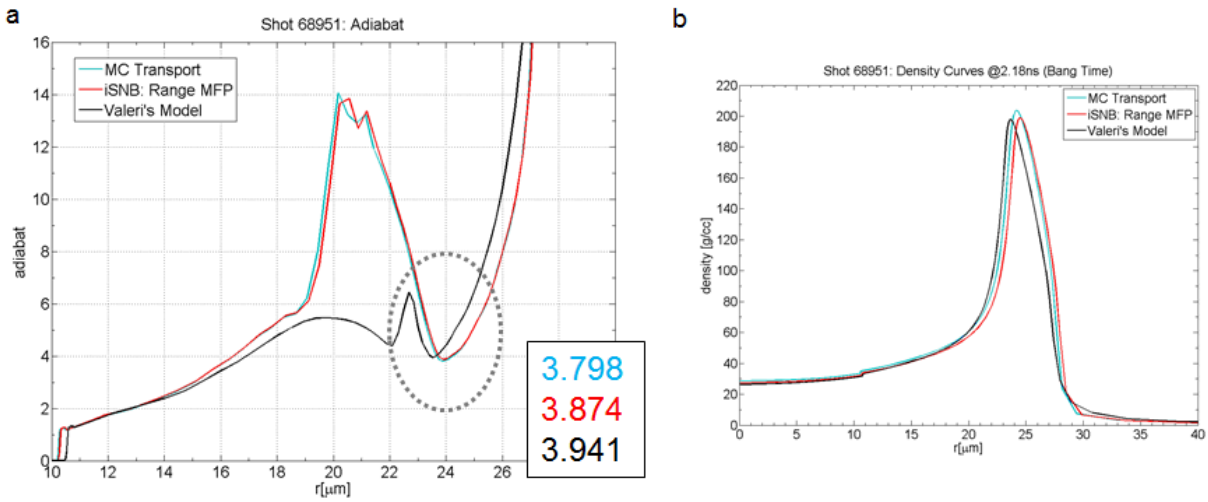

Figure 10. (**a**) Shot 68951 adiabat at bang time for MC transport iSNB and Goncharov's model. (**b**) Density curve for shot 68951 at bang time.

2D Simulations

***Shock timing experiment Omega shot 60303*:**

The 2D Omega shot 60303 simulation was run in LLE's 2D DRACO multiphysics code using the iSNB method and Chenhall's MC transport method. The MC transport model was run using 2.5×10^7 MCP per time step. The shock timing results for the MC transport and iSNB methods were quiet similar in the 2D simulation (Figure 11). Since the 2D simulation is largely

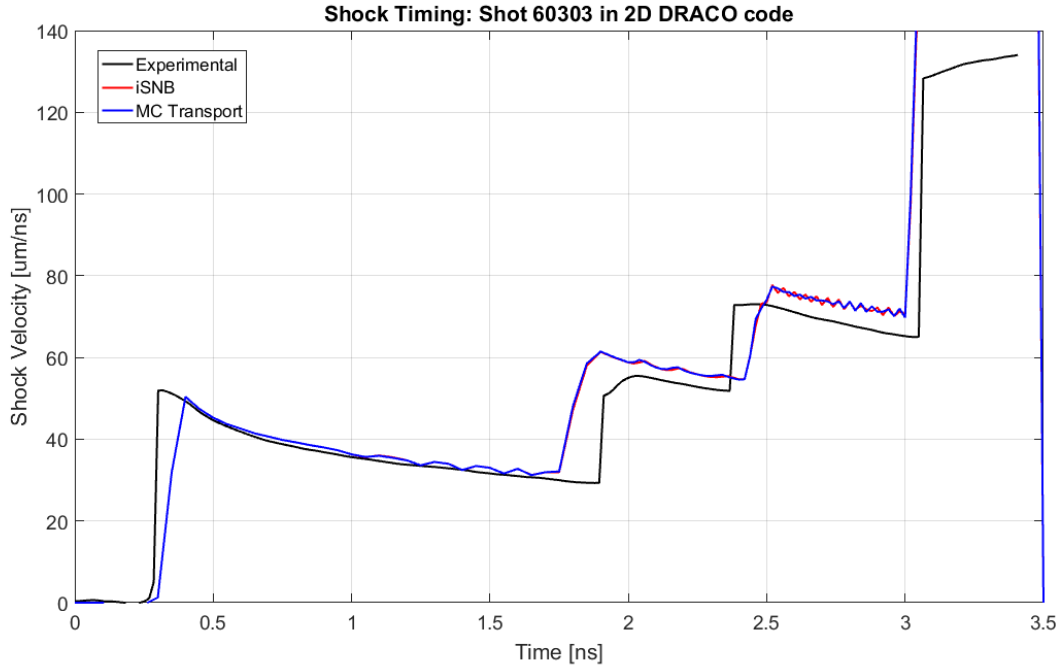

Figure 11. Comparison of shock timing in the iSNB and MC transport simulations of shot 60303 to experimental VISAR result [3].

spherically symmetric this is expected. In comparison to the 1D results the 2D result do a better job at matching the experimentally measured shock velocity prior to 1.8 ns. After 2 ns the 1D and 2D results largely predict the same shock velocity and timing. The earlier first shock convergence (near 1.9 ns) in the 2D simulation is a result of the lower predicted shock velocity which allows the second shock to catch up more quickly.

NIF phase plate polar direct drive design [5]:

The phase plate simulation was run in LLE's 2D DRACO method using the iSNB method and Chenhall's MC transport method. The MC transport model was run using 1.2×10^7 MCP per time step. Both the iSNB and MC simulations were run to 7.6 ns which is the end of the main laser drive. The electron temperature and density profiles taken along the z-axis (for ease of comparison) are compared for each model at 7.4ns (Figure 12).

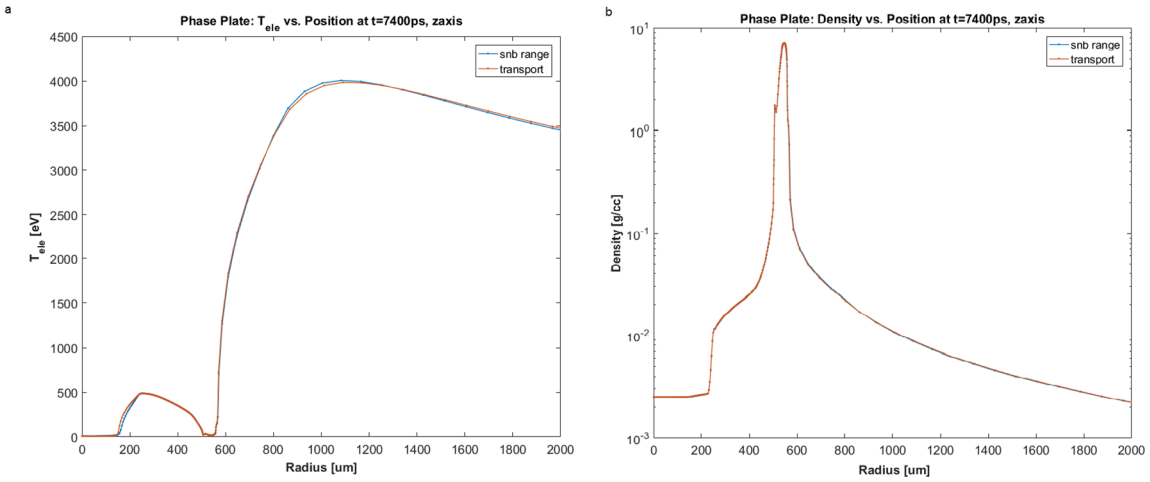

Figure 12. Electron temperature (a) and density (b) profile comparison for the NIF Phase Plate simulations for iSNB and MC transport methods.

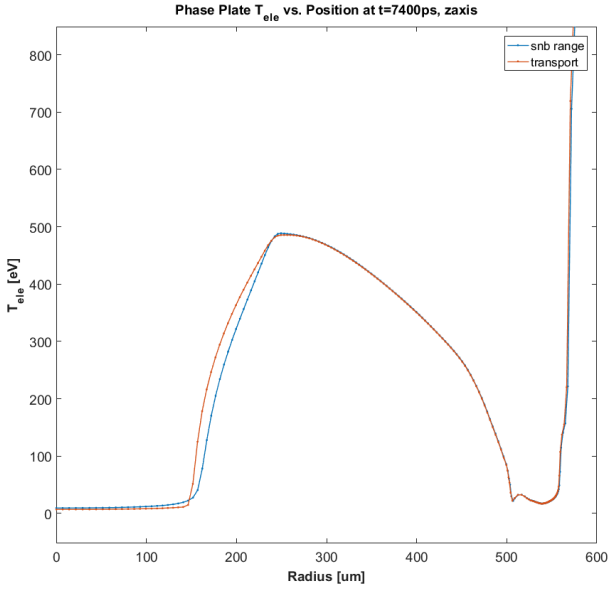

Figure 13. Electron temperature profiles for iSNB and MC transport simulations at 7400ps showing a decrease in preheating in the MC method at the inner shock front.

DISCUSSION:

In regards to the additional computational cost of the transport method, when using the same number of processors the MC transport method takes about an order of magnitude greater run time than the iSNB method when using about 10 MCP per cell/group. Furthermore, lower energy shots such as shot 60303 take less time to run than higher energy shots. This is because higher energy shots have higher average electron temperatures with longer associated MFP lengths increasing computational costs due to longer resultant particle histories.

***Shock timing experiment Omega shot 60303*:**
The shot 60303 iSNB and MC transport simulations gave nearly identical results for the shock timing in both the 1D and 2D simulations. This seems to indicate that transport effects do not have a large impact on the simulation of this problem. In addition, shot 60303 is a relatively low energy shot so there will be decreased effects from higher energy long MFP particles in comparison to higher energy shots. The other model, Goncharov's model, most closely matches the experimental result. However since Goncharov's method is limited to 1D a usable 2D transport model remains necessary.

***Cryogenic target implosion experiment Omega shot 68951*:**
The shot 68951 iSNB and MC transport simulations give very similar results to each other. The transport simulation had an adiabat 3.798 and the iSNB simulation a value of 3.874 a difference of only 2%. At both the 1.5 ns and 2.1 ns time steps the transport model has a slightly lower temperature at the origin. The lower origin temperature in the transport model is a likely sign that there is less preheating occurring out ahead of the implosion shell. This is to be expected

since the transport model use a finite range which limits the spread of particles versus the iSNB diffusion particle which allows "particles" to exponentially decay resulting in a longer effective range. Furthermore, the density profiles show that the transport model predicts a slightly more inwardly progressed shell. This can also be explained by a reduced preheating since a lower temperature means that there will be less resistance against the inward movement of the shell.

NIF phase plate polar direct drive design [5]:
The iSNB and MC transport simulations both produced similar results. At the 7.4 ns time step, the peak electron temperature is 3984 eV for the MC method and 4006 eV for the iSNB method. The peak density is 7.252 g/cm^3 for the MC method and 7.205 g/cm^3 for the iSNB. The outer corona temperature is 2967 eV for the MC method and 2872 eV for the iSNB. Furthermore, the temperature drops off more steeply for the MC method at the innermost shock surface indicating that less preheating is occurring (Figure 13). This is likely due to a range being used which has a sharp cutoff versus the iSNB diffusion solution which decays exponentially.

ANTICIPATED IMPACT:

Anticipated impact:
The anticipated impact of this work is higher fidelity modeling of the electron thermal heat flux within ICF simulations. The MC transport model offers several potential advantages over the iSNB diffusion model. First, continuous slowing down is not well modeled by diffusion theory. The transport model allows for better modeling of electron range as diffusion theory only allows for exponential solutions which do not allow for sharp cutoffs in the electron range.

Furthermore a MC method allows for the potential to have better EM modeling than a diffusion model. The iSNB model incorporates an electric field correction by modifying the MFP in the diffusion term. This is disadvantageous as this correction is not directionally dependent and only allows for additional slowing down of the particle to occur. A MC method on the other hand allows for modification to the particle trajectories due to EM field as well as allowing both up and down scattering of the particle depending on the particles relation to the EM field direction. Including the effects of these EM fields on the transport model are still on going, however a preliminary study with the electric field in 1D indicates that particle transport is most effected in regions of low densities.

Future work:
Future work will be focused on studying ways in which the MC transport and iSNB diffusion methods can be made to give greater difference in solution in order to better tease out the differences between the two methods. One pathway towards accomplishing this is to run a series of implosion simulations with varying levels of asymmetry in the laser drive. Since the MFP for the iSNB is computed only in the direction of the origin the transport method would be expected to reveal more transverse effects. Therefore a more asymmetric simulation could better ascertain the differences imparted by the higher order angular handling in the transport method.

Currently the transport method takes about an order of magnitude longer to run than the diffusion method when using the same number of computer cores. The diffusion method however is limited to a number of processors equal to the number of energy groups whereas the MC method has no such limitation. An alternative option to adding more processors for MC speed up is to hybridize the algorithm to allow it to use the diffusion method in cells where appropriate. Most likely this will be accomplished by using the faster iSNB method for cells/groups in which the relevant MFP is of an order smaller than the local gradient size. This would allow for a reduction in the total number of particles or allow for particles to be better allocated to regions where long MFP effects are particularly relevant. Another future work deals with the inclusion of electromagnetic fields within the particle transport. Based on an initial study, electric fields appear to have the most effect in low density high temperature regions such as the outer corona region.

CONCLUSION:

Overall, Chenhall's MC transport method is at least as accurate as the currently in use iSNB method. There is evidence that there is a small reduction in the preheating with the transport method versus the iSNB method. As the method currently stands however this small decrease in preheating alone does not seem to largely affect the simulation result and further study will be necessary to better characterize the circumstances with which the two models differ. These simulations will be run over the course of the next few months as Chenhall completes his PhD thesis work.

REFERENCES:

1. G. P. Schurtz, Ph. D. Nicolai, and M. Busquet. A nonlocal electron conduction model for multidimensional radiation hydrodynamics codes. Physics of Plasmas, 7(10), October 2000.
2. D. Cao, G.A. Moses, J. Delettrez. Improved non-local electron thermal transport model for two-dimensional radiation hydrodynamics simulations. Physics of Plasmas 22, 082308 (2015).
3. T. R. Boehly, V. N. Goncharov, W. Seka, S. X. Hu, J. A. Marozas, D. D. Meyerhofer, P.M. Celliers, D. G. Hicks, M. A. Barrios, D. Fratanduono, and G. W. Collins. Multiple spherically converging shock waves in liquid deuterium. Physics of Plasmas, 18, September 2011.
4. Omega shot 68951 LILAC input deck provide by J.A. Delettrez. Personal Communication (2015).
5. D. Cao et. al. A new intermediate far-field spot design for polar direct drive at the national ignition facility. BAPS DDP 57 (2015)
6. L. Spitzer, Jr. and R. Harm, Transport Phenomena in a Completely Ionized Gas. Physical Review 89, 977 (1953)
7. J. F. Luciani, P. Mora, and J. Virmont. Nonlocal heat transport due to steep temperature gradients. Physics Review Letter, 51(18), 1983.

8. S. Atzeni, A. Schiavi, and J.R. Davies. Stopping and scattering of relativistic electron beams in dense plasmas and requirements for fast ignition. Plasma Phys Control. Fusion 51, 015016 (2009)
9. T.J. Collins et.al. A polar drive ignition design for the National Ignition Facility. Physics of Plasmas 19, 056308 (2012)
10. W. Manheimer, D. Colombant, and V. Goncharov, Phys. Plasmas 15, 083103 (2008)

Sandia National Laboratories is a multi-program laboratory managed and operated by Sandia Corporation, a wholly owned subsidiary of Lockheed Martin Corporation, for the U.S. Department of Energy's National Nuclear Security Administration under Contract DE-AC04-94AL85000.